Microstructural Evaluation of Rare-Earth-Zinc Oxide-Based Varistor Ceramics

José Geraldo de Melo Furtado[a]*, Luiz Antônio Saléh*[a], *Eduardo Torres Serra*[b],

Glória Suzana Gomes de Oliveira[a], *Maria Cecília de Souza Nóbrega*[c]

[a]*Special Technologies Department, Electric Power Research Center, CEPEL,*
P. O. Box 68007, 21940-970 Rio de Janeiro, Brazil
[b]*R&D Directorate, Electric Power Research Center, CEPEL, Rio de Janeiro, Brazil*
[c]*Department of Metallurgical and Materials Engineering, Federal University of Rio de Janeiro,*
P. O. Box 68505, 21945-970 Rio de Janeiro, Brazil

Zinc oxide varistors are nonlinear voltage dependent ceramic resistors used to suppress and limit transient voltage surges. The work reported in this paper involves the relationship between microstructural characteristics and the varistor performance of ZnO ceramics doped with rare-earth oxides. Samples of these ceramics with different nonlinear current-voltage characteristics, according to the specific chemical composition and sintering parameters, were prepared and microstructurally analyzed by scanning electron microscopy, X-ray energy dispersive spectroscopy, X-ray fluorescence spectroscopy and X-ray diffraction. The results denote that intergranular phase is rich in rare-earth elements, but its morphology, obtained by selective leaching of ZnO grains (which are only doped with Co), provides evidence that ZnO grains are not completely surrounding by the intergranular phase, also existing ZnO grains are in direct contact with each other, as well as it occurs in conventional varistor system.

1. Introduction

Zinc oxide (ZnO) varistors (variable resistors) are polycrystalline ceramic devices exhibiting highly nonlinear (nonohmic) electrical behavior and greater energy absorption capabilities[1,2]. The fabrication of ZnO varistors is done by mixing semiconducting ZnO powder with other oxide powders such as Bi, Co, Mn, and Pr, and subjecting the powder mixture to conventional ceramic pressing and liquid-phase sintering techniques[3]. The sintering results in a polycrystalline ceramic with a singular grain boundary property which produces the nonlinear current-voltage (I-V) characteristics of the device[4]. Microstructurally, the ZnO varistors are comprised of semiconducting n-type ZnO grains, surrounded by very thin (1-10^{-3} μm) insulating intergranular layers[2,5]. Several conduction mechanisms for the varistor have been proposed based on this ceramic microstructure[1,2,6], which has led to varistor behavior being widely interpreted as resulting from the series-parallel network formed by the ZnO-intergranular-phase junctions[6,7]. Capacitance measurements as a function of voltage have supported the model of Schottky barriers at grain boundaries[8]. Electrically, the varistors show highly nonlinear I-V characteristics similar to the back-to-back Zener diode, but with much higher voltage, current, and energy handling capabilities[9]. As a result, they are widely used as surge absorbers in electronic circuits and core elements of surge arresters in electric power systems[10].

ZnO varistors are divided generally into two categories, called Bi_2O_3-based and Pr_6O_{11}-based varistors, in terms of varistor-forming oxides inducing the nonlinear properties of varistors[11]. Most of the commercial ZnO varistors are Bi_2O_3-based varistors, which have been mainly studied in various aspects since ZnO varistors were discovered by Matsuoka et al.[12]. However, Bi_2O_3-based ZnO varistors are not suitable to be used in multilayer chip varistors manufacture, due to Bi_2O_3 having a high volatility and reactivity[13]. Furthermore, in

general, Bi_2O_3-based ZnO varistors possess four phases, namely ZnO grains, Bi-rich intergranular layers, an additional insulating spinel phase, which does not play any role in electrical conduction, and pyrochlore phase. On the other hand, in Pr_6O_{11}-based ZnO varistors only two phases are present in a sintered body, namely, ZnO grains and the intergranular phase composed mainly of praseodymium oxide[14]. The absence of a spinel phase increases the active grain boundary through which the electrical current flows. Therefore, the effective cross-section area of the element is increased[13]. Earlier studies about Pr_6O_{11}-based varistors have been limited to the ternary system ZnO-Pr_6O_{11}-CoO and dissimilarities between Bi_2O_3-based and Pr_6O_{11}-based ZnO varistors[11,15-18]. Recently, many works have been made in order to study the influence of other rare-earth oxides (such as Y_2O_3, Nd_2O_3, Er_2O_3, and Dy_2O_3) on the microstructural and electrical properties of the ternary system ZnO-Pr_6O_{11}-CoO[5,13,19]. The varistors produced have exhibited a relatively good electrical performance[13,19].

Earlier studies in ZnO varistors have shown that the narrow regions, where the sintered grains have grown together, control the resistance of the entire sample[12,20]. In those regions, the surface/volume ratio is sufficiently high for the acceptor concentration (which occurs because of adsorbed oxygen) to exceed the donor concentration inside the ZnO grains[21]. More recent works have shown that Schottky barriers result from interface states because of the chemisorbed oxygen ion at the ZnO-ceramic grain boundaries[1,2,22-25]. Although the microstructure of varistors exhibit considerable variation from one manufacturer to another, they all exhibit the characteristics of a typical ceramic prepared by liquid-phase sintering, consisting mainly of large ZnO grains with a varistor former-rich second phase at the nodal points (triple juntions) and/or intergranular layer (IGL) regions. In the present work an evaluation of the microstructural features of

*e-mail: furtado@cepel.br

ZnO-Pr_6O_{11}-Nd_2O_3-Co_3O_4-Cr_2O_3 based varistor ceramics (ZPNC) was made and applied to the understanding of the varistor performance.

2. Experimental

Appropriate molar reagent grades of ZnO (Merck), Co_3O_4 (Riedel), Pr_6O_{11} (Aldrich), Nd_2O_3 (Aldrich), Cr_2O_3 (Merck) powders were used to prepare the ZnO based ceramics. The sample compositions are shown in Table 1. The powders with adequate compositions were ball milled with zirconia balls in isopropyl alcohol media inside of a zirconia jar for 24 hours. The resultant mixture was dried at 110 °C for 12 hours and calcined in air at 750 °C for 2 hours. The calcined mixture was granulated in a 200 mesh sieve and pressed into discs of 12.4 mm in diameter and 2.1 mm in thickness at a pressure of 80 MPa. The discs were sintered at 1300-1350 °C with interval by 25 °C in air atmosphere for 1 hour. The heating and cooling rates were 6 °C/min. The average size of the final samples was 10.2 mm in diameter and 1.1 mm in thickness. The sintered bodies were sanded and polished, silver paste was coated on both faces of the samples and the silver electrode was formed by heating at 600 °C for 10 min. The area of the electrodes was approximately 0.212 cm^2. The I-V characteristics of ceramics were measured using a curve tracer source-measurement unit (Tektronix 577). The breakdown electric field (E_B) was measured at 1.0 mA/cm^2 and the leakage current density (J_L) was measured at 80% of breakdown electric field. In addition, the nonlinear coefficient (α) was estimated for current-density ranges of 1.0-10.0 mA/cm^2.

The sample microstructures were examined by scanning electron microscopy (SEM, ZEISS DSM 960) applied on the polished and 6 M-NaOH aqueous solution-etched (5 minutes) surface of samples, as well as on the fractured surface of ZPNC samples. The grain sizes were estimated by linear intercept method[26]. The compositional analysis of the selected areas was determined by an attached X-ray energy dispersive spectroscopy (EDS, Oxford ISIS) system. The density (ρ) of the ZPNC ceramics was measured by the Archimedes method. The crystalline phases were identified by powder X-ray diffraction (XRD, Diano XRD-8545, $\lambda CuK\alpha$ radiation). The chemical composition of the residue of leached ZPNC samples was determined by X-ray fluorescence (XRF, 3070 Rigaku spectrometer). The leaching procedure consisted of placing each sample into a beaker containing 400 mL of solution (cf. Table 3 for solution systems used) under constant agitation. After each specific dissolution time, the residue was passed through a preweighed millipore filter, dried and reweighed. The weight percent of the residue was calculated.

3. Results and Discussion

The Table 2 presents the results obtained (varistor characteristics) from electrical measurements of the ZPNC samples and the Figure 1 shows the microstructural parameters evaluated for this varistor ceramic system in function of the chemical composition and sintering temperature employed. Figure 2 shows microstructure of

Table 1. Composition of investigated samples of the ZPNC system.

Sample	Composition (mol %)				
	ZnO	Pr_6O_{11}	Nd_2O_3	Co_3O_4	Cr_2O_3
ZPNC-1	97.4	0.5	1.0	1.0	0.1
ZPNC-2	97.3	0.5	1.0	1.0	0.2
ZPNC-3	96.5	0.8	1.5	1.0	0.2

Table 2. Varistor characteristics of investigated samples of the ZPNC system.

Sintering Temperature (°C)	Varistor Characteristics[1,2,3]								
	ZPNC-1			ZPNC-2			ZPNC-3		
	α	E_B	J_L	α	E_B	J_L	α	E_B	J_L
1300	51.2	5.8	28.6	54.9	6.2	30.5	47.1	5.6	49.5
1325	56.4	3.5	26.2	62.4	3.6	17.2	46.5	2.9	39.1
1350	33.0	2.2	23.7	34.2	2.4	20.8	18.7	1.6	32.9

[1] E_B (kV/cm) and J_L ($\mu A/cm^2$).
[2] Mean of the five samples.
[3] Average discrepancy (δ) (all samples): $\delta\alpha \cong 0.6\%$; $\delta E_B \cong 0.8\%$; $\delta J_L \cong 1.2\%$.

Table 3. Results of residue analysis (XRF) of the leached ZPNC samples[1].

Etchant Solution	Dissolution Time (h)	Weight (%) (wt. (%))	Rare-earth oxides (wt. (%))	Transit. Elem. oxides (wt. (%))
			ZPNC-1 / ZPNC-2 / ZPNC-3	
5% PAAS[2]	24	8.9 / 9.0 / 12.2	81 / 81 / 80	19 / 19 / 20
10% PAAS	24	8.6 / 8.8 / 11.8	82 / 82 / 81	18 / 18 / 19
20% PAAS	24	7.2 / 7.2 / 9.9	85 / 84 / 82	15 / 16 / 18
50% PAAS	24	6.9 / 6.9 / 9.4	86 / 85 / 84	14 / 15 / 16
10% PAEthS[3]	48	11.2 / 11.3 / 15.2	79 / 80 / 79	21 / 20 / 21
20% PAEthS	48	10.4 / 10.5 / 14.1	81 / 81 / 80	19 / 19 / 20
50% PAEthS	30	10.1 / 10.1 / 13.8	82 / 82 / 81	18 / 18 / 19
Mean Value (20% PAAS and 50% PAAS)			84	16
Mean Value (20% PAEthS and 50% PAEthS)			81	19

[1] Samples sintered at 1325 °C.
[2] PAAS: perchloric acid aqueous solution.
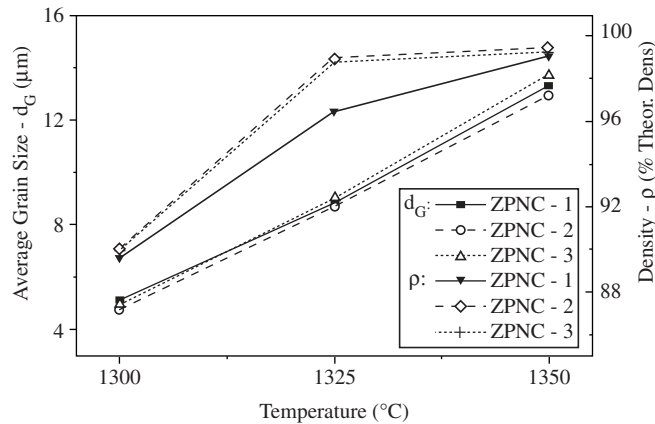[3] PAEthS: perchloric acid/ethanol solution (3:2, vol/vol).

Figure 1. Average Grain Size and Relative Density (in percentage of the theoretical density) of ZPNC varistor ceramics as a function of the sintering temperature.

(a)

(b)

(c)

the fractured surface examined by SEM of ZPNC samples sintered at 1325 °C. Among all the samples analyzed, the ZPNC-2 sintered at 1325 °C exhibited better varistor performance, i. e., $\alpha > 60$ and low leakage current in the prebreakdown regime. As the sintering temperature increases, the average grain size (d_G) was increased in the range of 5.1-13.3 µm for ZPNC-1 samples, 4.8-12.9 µm for ZPNC-2, and 5.0-13.7 µm for ZPNC-3. This increase of grain size resulted in the decrease of the breakdown electric field (cf. Table 2). The relative density of ZPNC ceramics was increased in the range of 5.03-5.56 g/cm^3 for ZPNC-1 subsystem, 5.05-5.58 g/cm^3 for ZPNC-2, and 5.05-5.57 g/cm^3 for ZPNC-3. In general, all the samples present satisfactory densification level (in the range of 89.7% to 99.5% of the theoretical density, 5.61 g/cm^3) and stability of the nonlinear electrical characteristics. The increase of Cr_2O_3 content improves the nonlinear coefficient and the electric breakdown field, in all sintering temperature evaluated. For the samples sintered at 1300 °C, the increase of Cr_2O_3 content resulted in increase of the leakage current, but for the samples sintered at 1325 °C and 1350 °C resulted in the decrease of the leakage current. In fact, the added Cr_2O_3 (0.2 mol%) resulted in the improving of the varistor behavior of the quaternary system $ZnO-Pr_6O_{11}-Nd_2O_3-Co_3O_4$ proposed by Nahm et al.[5]. In all sintering temperature studied, the increase of rare-earth oxides content resulted in the degeneracy of the varistor properties.

The Figure 3 shows the XRD patterns of ZPNC ceramic samples, identifying the ZnO phase (grains), Pr_6O_{11} and Nd_2O_3 rich phase peaks. The Pr and Nd oxides coexist in the grain boundaries, intergranular layers (IGL) and in nodal points, behaving as a single phase[5,13]. Figure 4a shows a SEM micrograph of the polished and chemical etched surface (leached) of the ZPNC-2 ceramic sintered at 1300 °C and Figure 4b shows in detail the X-Z-marked region. The X, Y and Z marks (Figure 4) indicate the specific regions to qualitative EDS analyses (Figure 5), denoting, respectively, a ZnO grain, a very thin IGL (grain boundaries region) and an IGL region, whose EDS patterns are shown, respectively, in the Figures 5a, 5b and 5c. In Figure 5c can be seen that, in fact, the IGL region contains a high concentrations of rare-earth elements (Pr and Nd) and smaller amounts of Cr and Co. However, as can be seen in the Figures 5 and 6, the intergranular layer distribution is heterogeneous, because regions exist that ZnO grains are in direct contact with each other (cf. Figure 6). The microstructures present in Figures 2 and 4 are not quite uniform but a bimodal grain size distribution was not observed in any of the samples. The heterogeneous distribution of the Pr-Nd-rich intergranular material observed, mainly in Figure 4, suggests
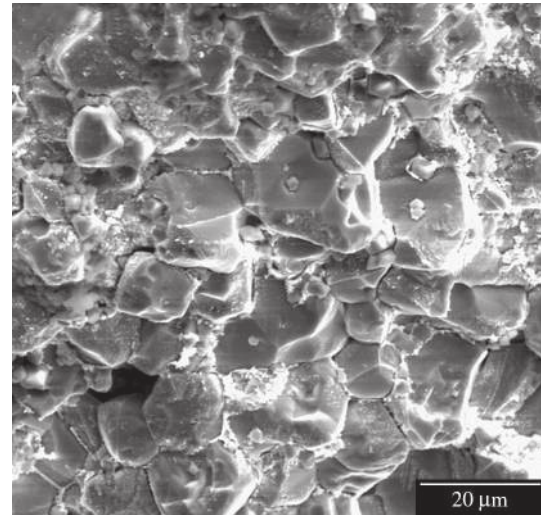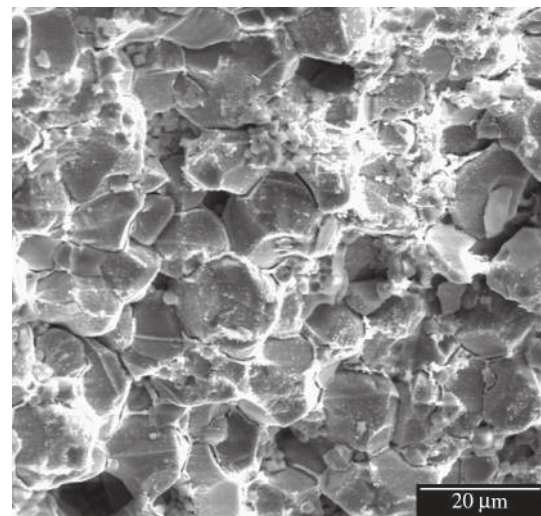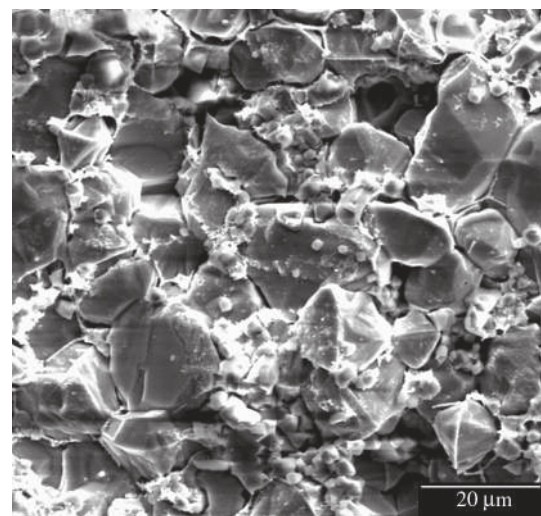
Figure 2. SEM micrographs of the fractured surface of the ZPNC samples sintered at 1325 °C: a) ZPNC-1; b) ZPNC-2; and c) ZPNC-3 (bar = 20 µm).
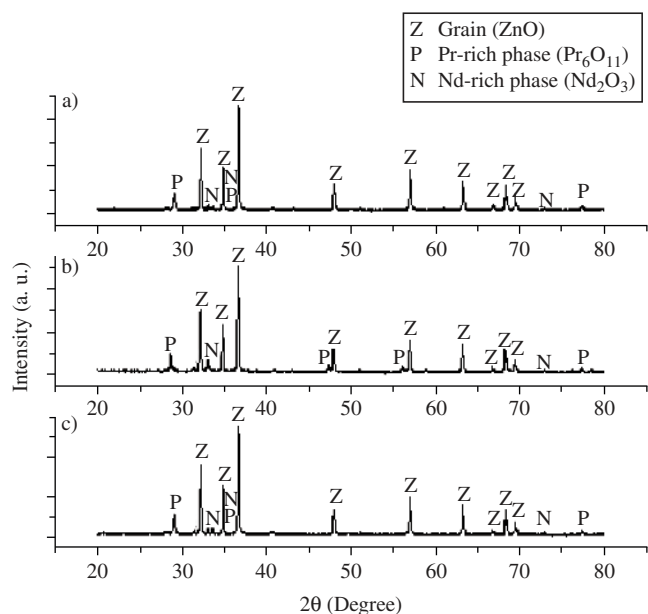
Figure 3. X-ray diffraction (XRD) patterns of ZPNC varistor ceramics: a) ZPNC-1; b) ZPNC-2; and c) ZPNC-3. Reference pattern codes for rare-earth oxides (PDF index name): 00-024-1006 (praseodymium oxide) and 00-043-1023 (neodymium oxide).
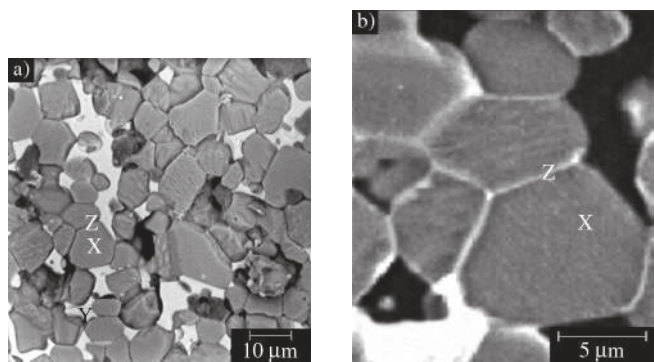

Figure 4. a) SEM micrograph of the polished and etched surface of the ZPNC-2 ceramic sintered at 1300 °C; and b) X-Z-marked region in detail.

Figure 5. EDS analysis of ZPNC-2 varistor ceramic: a) ZnO grain (X-marked, Figure 4a); b) Grain Boundary region (Z-marked, Figure 4a) and c) IGL region (Y-marked, Figure 4a).

Figure 6. SEM micrograph of magnified detail of the ZPNC-2 microstructure showing that ZnO grains are in direct contact with each other.

that processing conditions are not optmized yet, and the ZnO grains were not suffered an uniform wetting by liquid phase-varistor former rare-earth mixture, although the resultant varistor ceramic samples have presented excellent electrical performance (cf. Table 2). In fact, the uniform distribution of grain boundary materials (varistor formers and dopants) can be expected to improve significantly the performance of ceramics which are liquid-phase sintered and this is believed to result in the proper conditioning required to form the electrically active junctions in the large majority of the grain boundary regions such as shown the enlarged SEM micrograph of the triple point of the ZPNC-2 sample (Figure 6)[2,16]. Thus, from these observations, it is reasonable that the nonlinear electrical behavior of ZPNC ceramics can be considerablly improved by means of the increase of its microstructural homogeneity.

A quantitative residue analysis, by XRF, using perchloric acid solutions (cf. Table 3), which are most effective in the selective leaching of the ZnO grains, showed that the residue is formed mainly by rare-earth oxides (about 80 wt. (%)), which exhibited, by EDS analysis, the typical composition of a solidified eutectic liquid charac-
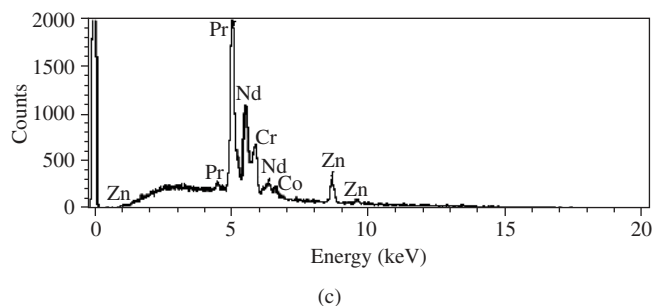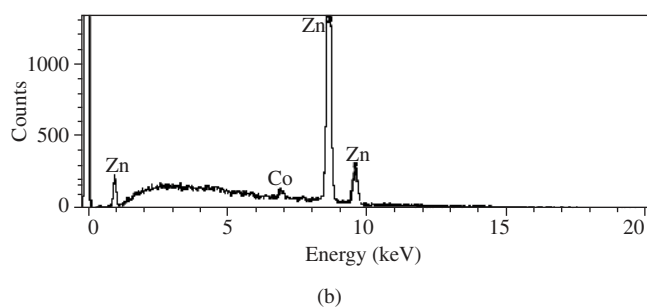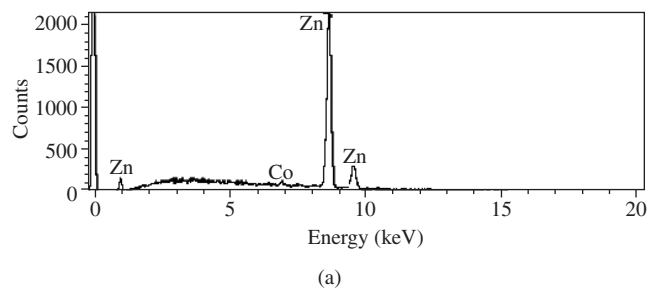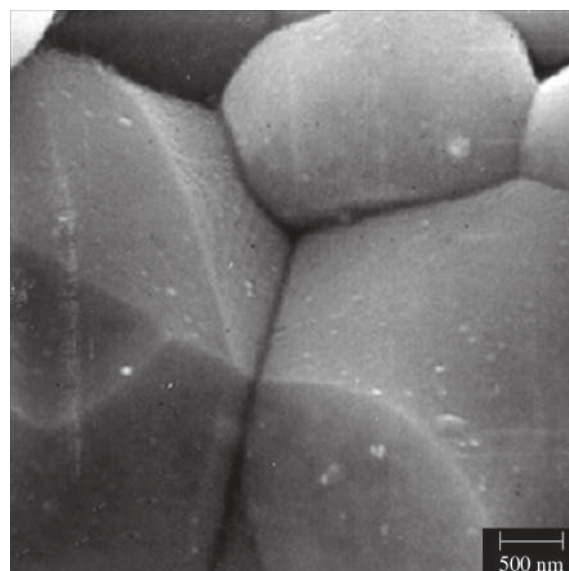
teristic of the ZnO-Pr_6O_{11}-Co_3O_4 system (82 wt. (%) Pr_2O_3-10 wt. (%) CoO-8 wt. (%) ZnO, consisting in the praseodymium rich phase)[16,17] doped with Nd_2O_3. Pr_6O_{11} and Co_3O_4 present variable stoichiometry with oxygen, depending on oxygen partial pressure and temperature conditions, so that Pr_2O_3 is formed during the sintering process by reduction of the Pr_6O_{11}[11].

4. Conclusions

The microstructure of ZnO-Pr_6O_{11}-Nd_2O_3-Co_3O_4-Cr_2O_3 based varistor ceramics (ZPNC) consists of two phases: ZnO grains (doped with Co) and rare-earth elements (Pr and Nd)-rich phase (doped with Cr and Co) segregated at grain boundaries. The distribution of the intergranular layer is heterogeneous and exist ZnO grains that are in direct contact. Additionally, ZPNC ceramics sintered at 1325 °C with 0.2 mol% Cr_2O_3 exhibited the most excellent varistor characteristics.

References

1. Gupta T. Application of zinc oxide varistors. *Journal of the American Ceramic Society*. 1990; 73(7):1817-1840.

2. Clarke D. Varistor ceramics. *Journal of the American Ceramic Society*. 1999; 82(3):485-502.

3. Lagrange A. Present and future of zinc oxide varistors. In: Steele B, editor. *Electronic Ceramics*. revised ed. London: Elsevier Applied Science; 1991.

4. Santos J, Longo E, Leite E. Model for zinc oxide varistor. *Journal of Materials Research*. 1998; 13(5):1152-1157.

5. Nahm C, Park C, Yoon H. Microstructure and varistor properties of ZnO-Pr_6O_{11}-CoO-Nd_2O_3 based ceramics. *Journal of Materials Science Letters*. 2000; 19(4):271-275.

6. Blatter G, Greuter F. Carrier transport through grain boundaries in semiconductors. *Physical Review B: Condensed Matter and Materials Physics*. 1986; 33(6):3952-3966.

7. Eda K. Electrical properties of Zn-Bi_2O_3 metal oxide heterojunction – a clue of a role of intergranular layers in ZnO varistor. In: Leamy H., editor. *Grain Boundaries in Semiconductors*. revised ed. London: Elsevier Applied Science; 1991.

8. Mantas P, Baptista J. The barrier height formation in ZnO varistors. *Journal of the European Ceramic Society*. 1995; 15(7):605-615.

9. Levinson L, Philipp H. The physics of metal oxide varistors. *Journal of Applied Physics*. 1975; 46(3):1332-1341.

10. Eda K. Zinc oxide varistors. *IEEE Electrical Insulation Magazine*. 1989; 5(6):28.

11. Mukae K. Zinc oxide varistors with praseodymium oxide. *American Ceramic Society Bulletin*. 1987; 66(9):1329.

12. Matsuoka M. Nonohmic properties of zinc oxide ceramics. *Japanese Journal of Applied Physics Supplement*. 1970; 10(6):736-742.

13. Nahm C. The electrical properties and d.c. degradation characteristics of Dy_2O_3 doped Pr_6O_{11}-based ZnO varistors. *Journal of the European Ceramic Society*. 2001; 21(4):545-553.

14. Chun S, Wakiya N, Funakubo H, Shinozaki K, Mizutani N. Phase diagram and microstructure in the ZnO-Pr_2O_3 system. *Journal of the American Ceramic Society*. 1997; 80(4):995-998.

15. Mukae K, Tsuda K, Nagasawa I. Non-ohmic properties of ZnO-rare earth metal oxide-Co_3O_4 ceramics. *Japanese Journal of Applied Physics*. 1977; 16(8):1361-1368.

16. Alles A, Burdick V. The effect of liquid-phase sintering on the properties of Pr_6O_{11}-based ZnO varistors. *Journal of Applied Physics*. 1991; 70(11):6883-6890.

17. Alles A, Burdick V, Puskas R, Callahan G. Compositional effects on the liquid-phase sintering of praseodymium oxide-based zinc oxide varistors. *Journal of the American Ceramic Society*. 1993; 76(12):2098-2102.

18. Lee Y, Liao K, Tseng T. Microstructure and crystal phase of praseodymium oxide in zinc oxide varistor ceramics. *Journal of the American Ceramic Society*. 1996; 79(9):2379.

19. Nahm C, Park C. Microstructure, electrical properties, and degradation behavior of praseodymium oxides-based zinc oxide varistors doped with Y_2O_3. *Journal of Materials Science*. 2000; 35(12):3037.

20. Selim F, Gupta T, Hower P, Carlson W. Low-voltage ZnO varistor: Device process and defect model. *Journal of Applied Physics*. 1980; 51(1):765.

21. Yan M. Microstructural control in the processing of electronic ceramics. *Materials Science and Engineering*. 1981; 48(1):53.

22. Tomlins G, Routbort J. Oxygen diffusion in single-crystal zinc oxide. *Journal of the American Ceramic Society*. 1998; 81(4):869.

23. Nóbrega M, Mannheimer W. Varistor performance of ZnO based ceramics related to their densification and structural development. *Journal of the American Ceramic Society*. 1996; 79(6):1504.

24. Zu P, Tang Z, Wong G, Kawasaki M. Ultraviolet spontaneous and stimulated emissions from ZnO microcrystallite thin films at room temperature. *Solid State Communications*. 1997; 103(8):459.

25. Ohnishi T, Ohtomo A, Kawasaki M, Koinuma H. Determination of surface polarity of *c*-axis oriented ZnO films by coaxial impact-collision ion scattering spectroscopy. *Applied Physics Letters*. 1998; 72(7):824.

26. Mendelson M. Average grain size in polycrystalline ceramics. *Journal of the American Ceramic Society*. 1969; 52(8):443.